

Article

A Compact CSRR-Based Sensor for Characterization of the Complex Permittivity of Dielectric Materials

Jurgen K. A. Nogueira *, João G. D. Oliveira , Samuel B. Paiva , Valdemir P. Silva Neto 
and Adaildo G. D'Assunção 

Department of Communication Engineering, Federal University of Rio Grande do Norte, Caixa Postal 1655, Natal 59078-970, Brazil; gjoao187@gmail.com (J.G.D.O.); samuel.b.paiva@hotmail.com (S.B.P.); vpraxedes.neto@gmail.com (V.P.S.N.); adaildo@ct.ufrn.br (A.G.D.)

* Correspondence: jurgenazevedo@hotmail.com; Tel.: +55-84-996670193

Abstract: A sensor is proposed to characterize the complex permittivity of dielectric materials in a non-destructive and non-invasive way. The proposed sensor is based on a rectangular patch microstrip two-port circuit with a complementary split-ring resonator (CSRR) element. The slotted CSRR element of the sensor plays a key role in determining the electrical properties of the materials under test (MUT). The sensitivity analysis is determined by varying the permittivity of the MUT. The proposed sensor is simulated and analyzed using Ansoft HFSS software. A prototype was fabricated and measurements were made on two different samples of dielectric materials with complex permittivity values available in the literature. The simulated and measured results showed good agreement.

Keywords: sensor; CSRR; dielectric characterization; complex permittivity; dielectric constant; tangent loss



Citation: Nogueira, J.K.A.; Oliveira, J.G.D.; Paiva, S.B.; Neto, V.P.S.; D'Assunção, A.G. A Compact CSRR-Based Sensor for Characterization of the Complex Permittivity of Dielectric Materials. *Electronics* **2022**, *11*, 1787. <https://doi.org/10.3390/electronics11111787>

Academic Editors: Yasir Al-Yasir, Chan Hwang See and Bo Liu

Received: 19 April 2022

Accepted: 23 May 2022

Published: 4 June 2022

Publisher's Note: MDPI stays neutral with regard to jurisdictional claims in published maps and institutional affiliations.



Copyright: © 2022 by the authors. Licensee MDPI, Basel, Switzerland. This article is an open access article distributed under the terms and conditions of the Creative Commons Attribution (CC BY) license (<https://creativecommons.org/licenses/by/4.0/>).

1. Introduction

Planar devices have increasingly attracted the attention of researchers looking to make improvements to their resources, as well as looking for applications in several technology areas. Planar microwave sensors have demonstrated important functionality in several applications, such as the food sector, industries, biomedical and microfluids [1–9]. Microwave sensors have several advantages: low cost, ease of fabrication, possibility of integration with other devices, and allowing the analysis of materials under test (MUT) in a non-destructive and non-invasive way, simplifying their characterization.

Recently, in planar sensors, elements based on resonators, such as the split-ring resonator (SRR) or the complementary split-ring resonator (CSRR), have been preferred, as they become more sensitive to change in the permittivity of the material under test (MUT) sample [10]. In recent studies, CSRR has been used for studies on the relative permittivity of solid, liquid and sandy soils [11–13], and in the characterization of the complex permittivity of dielectric materials [14–17]. In [11], a circular patch antenna with CSRR was used to investigate the percentage of water and to characterize two soil samples: quartz sand and red clay. In [12], a microfluidic microwave sensor for the analysis of small amounts of liquids is proposed. A sensor for detecting adulteration in liquids, such as mineral oil, is studied in [13]. The characterization of the complex permittivity was investigated in [14]. A microstrip filter was proposed, as a sensor, for the characterization of the relative permittivity and loss tangent of solid materials, by inserting a slotted CSRR on the filter's ground plane. In [15], a sensor based on a slotted CSRR is used for the complete characterization of magneto-dielectric materials. In addition to the complex permittivity, characterization of the relative permeability and the magnetic loss tangent was carried out.

Substrate integrated waveguide (SIW) technology was used in [16] to design an active sensor. Through the implementation of a CSRR, it was possible to obtain in two areas of

sensitivity: complex permittivity and permeability. In [17], two sensors based on CSRR were designed to characterize complex permittivity and permeability. The first sensor has a single sensitivity area for measurement. The second sensor has two CSRRs inserted for the simultaneous measurement of complex permittivity and permeability.

A sensor using the SRR resonator is proposed in [18] to detect the relative permittivity of solid dielectrics. A pair of identical SRRs is used on the sides of the microstrip line of the two-port circuit. Other resonant elements are also used to characterize dielectric materials, such as the interdigital capacitor, reported in [19] for the characterization of the relative permittivity of several solid samples. In [20], a microwave sensor was proposed based on the interdigital capacitor (IDC) for measuring the complex permittivity and material thickness. A structure using the compact microstrip resonant cell (CMRC) is presented in [21], to characterize the permittivity of dielectric materials, using a controlled oscillator and incorporated into a frequency synthesizer. The permittivity of the dielectric is measured through the voltage deviation. In [22], a differential sensor is proposed using two microstrip lines and both terminated with LC resonators, allowing two solid samples to be measured at the same time.

In this work, a planar microstrip two-port circuit is proposed based on the insertion of a CSRR in its patch, to improve the sensitivity of the device and, consequently, the measurement of the complex permittivity of different dielectric materials. The sensitivity of this device is analyzed by placing the MUT over the patch and is verified by the displacement of the resonance frequency. The simulation was performed using Ansoft HFSS software. Two dielectric materials were investigated: FR-4 fiberglass and glass samples. A prototype was fabricated and measured for the characterization of MUTs. The main contributions of this work are related to the development of a microwave sensor using CSRR with a new element geometry, compact size, high sensitivity, and accurate complex relative permittivity measurement results. Results are shown for the complex relative permittivity, sensitivity and size of the proposed sensor. Good agreement is observed between the simulated and measured results.

2. Materials and Methods

2.1. Theory and Principle of Operation

A two-port circuit is used to analyze the transmission coefficient (S_{21}) from port 1 (input) to port 2 (output). With the slotted CSRR element in the conducting patch, and with the permittivity change in the environment close to the CSRR, when inserting/placing the MUT sample, there is a change in the frequency response and in the magnitude of S_{21} . Equation (1) is used to relate the variation in the resonance frequency to the change in the properties of the analyzed material [11,14].

$$\frac{\Delta f_r}{f_r} = \frac{\int_v (\Delta \varepsilon E_1 \cdot E_0 + \Delta \mu H_1 \cdot H_0) dv}{\int_v (\varepsilon_0 |E_0|^2 + \mu_0 |H_0|^2) dv} \quad (1)$$

where Δf_r is the variation in the resonance frequency, $\Delta \varepsilon$ is the variation in permittivity, $\Delta \mu$ is the variation in permeability, E_0 and E_1 are the electric field distributions without and with the MUT sample, respectively, H_0 and H_1 are the magnetic field distributions without and with the MUT sample, respectively, and v is the disturbed volume.

2.2. Sensitivity Analysis

To analyze the sensitivity of the proposed sensor, it is necessary to obtain the variation in resonance frequency (Δf_r) and the variation in the permittivity of the MUT ($\Delta \varepsilon_r$); the ratio between them allows us to determine the sensitivity of the device. In order to compare criteria with other current sensors available in the literature, the normalized sensitivity (S_f) is used. The equations are presented in (2) and (3) [5,7,11,19,23].

$$S = \frac{\Delta f_r}{\Delta \varepsilon_r} = \frac{f_{ru} - f_{rl}}{\varepsilon_{ru} - \varepsilon_{rl}} \text{ (MHz)} \quad (2)$$

$$S_f = \frac{\Delta f_r}{(f_0)(\Delta \epsilon_r)} (\%) \tag{3}$$

where f_{ru} is the resonance frequency of the proposed sensor without the MUT samples (unloaded), f_{rl} is the resonance frequency of the proposed sensor with the MUT samples (loaded), ϵ_{ru} is the relative permittivity of the analyzed environment without the MUT samples, ϵ_{rl} is the relative permittivity of the environment with the MUT samples, and f_0 is the operating frequency of the sensor.

2.3. Design and Modeling of Sensor

The proposed sensor was modeled based on the basic theory of the microwave planar two-port circuit. The initial structure basically consists of an element that implements the impedance hopping method. With this type of modeling, it was necessary to add an element that would increase the sensitivity level of the circuit, and the chosen element was a complementary split-ring resonator (CSRR), which is a classic element for the area of sensors. Figure 1 shows the modeling in lossless transmission lines of the proposed device.

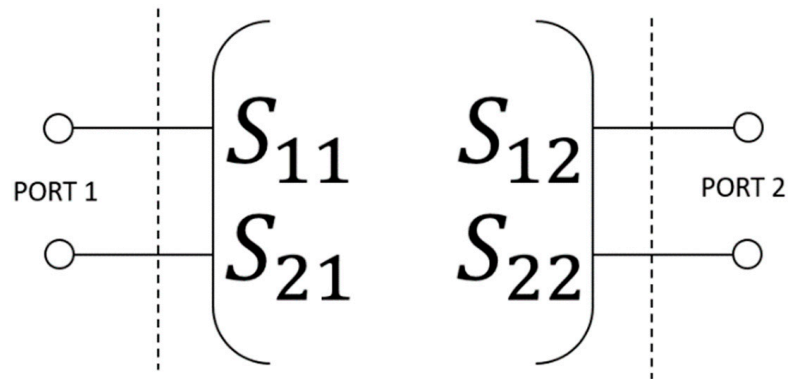


Figure 1. Modeling of the proposed circuit geometry assuming lossless transmission line sections.

In this way, the final element applied as a sensor is shown in Figure 2, with the device being implemented to reduce the dimensions of the device by placing the output port with a 90° axis orientation with respect to that of the input port. The device dimensions are shown in Table 1.

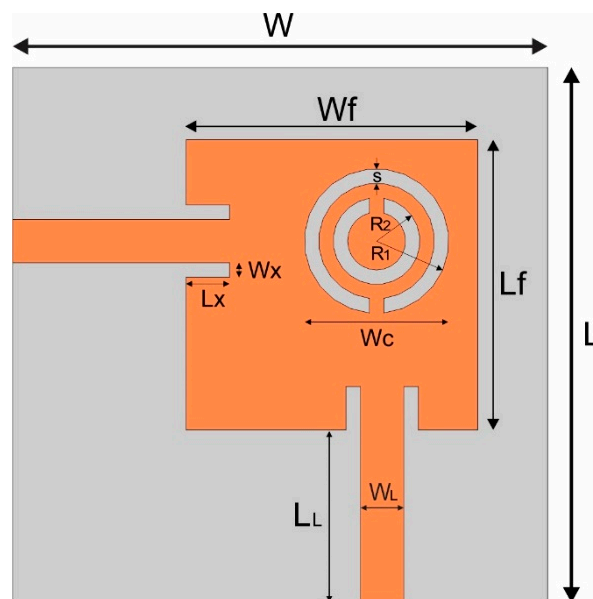


Figure 2. Top view of the proposed microstrip planar circuit geometry on an FR-4 dielectric substrate.

Table 1. Proposed microstrip circuit dimensions.

| Parameter | Value (mm) | Parameter | Value (mm) |
|----------------|------------|----------------|------------|
| W | 37 | W _c | 10 |
| L | 37 | W _x | 1 |
| W _f | 20 | L _x | 3 |
| L _f | 20 | R ₁ | 5 |
| W _L | 3 | R ₂ | 3 |
| L _L | 12 | s | 1 |

The equivalent circuit of the microwave sensor presented in Figure 2 is shown in Figure 3.

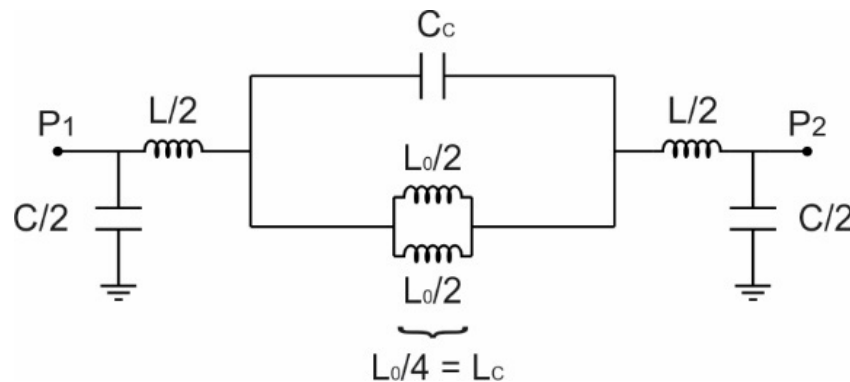


Figure 3. Equivalent circuit model of the proposed sensor.

The sensor is composed of a pair of orthogonal microstrip transmission lines loaded with a CSRR inserted in a central element between them. In the equivalent circuit model, L and C represent the inductance and capacitance of the microstrip transmission lines, respectively. In addition, two fundamental parameters for the analysis of the resonant frequency of the sensor are the capacitance C_c and the inductance L_c , which represent the capacitance and inductance of the CSRR unit cell, respectively. Then, as demonstrated by [24], the lumped circuit model presented in Figure 3 has a resonant frequency as given by Equation (4).

$$f_r = \frac{1}{2\pi\sqrt{L_c C_c}} \tag{4}$$

As mentioned previously, to improve the sensitive characteristics of the sensor, a CSRR was implemented in the central element; the total capacitance C_c of this element is greatly affected by the electrical characteristics close to the slotted CSRR element, due to its aperture characteristic, thus justifying its implementation for the detection of the dielectric constant of materials. The capacitance C_c is obtained using Equation (5) [12].

$$C_c = C_0 + \epsilon_{SUP} C_e \tag{5}$$

where C_0 describes the capacitance between the conductive plates and the circuit dielectric, and the term $\epsilon_{SUP} C_e$ describes the capacitive effect of the environment due to the superstrate placed on the CSRR.

Positioning of CSRR

An analysis was performed to find the best position of the CSRR inserted in the two-port circuit. Figure 4 shows the three positions analyzed. Figure 5 shows the simulated results of the transmission coefficient (S_{21}) as a function of frequency. The slotted CSRR element position that presented the best level of rejection was position 3 (Figure 4c), which was chosen to be used in this work.

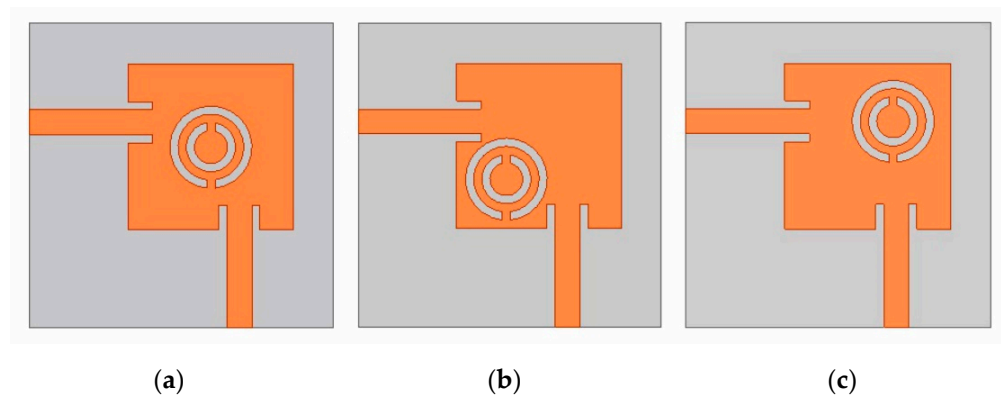


Figure 4. Three different CSRR element positions on the proposed microstrip planar circuit patch: (a) position 1, (b) position 2 and (c) position 3.

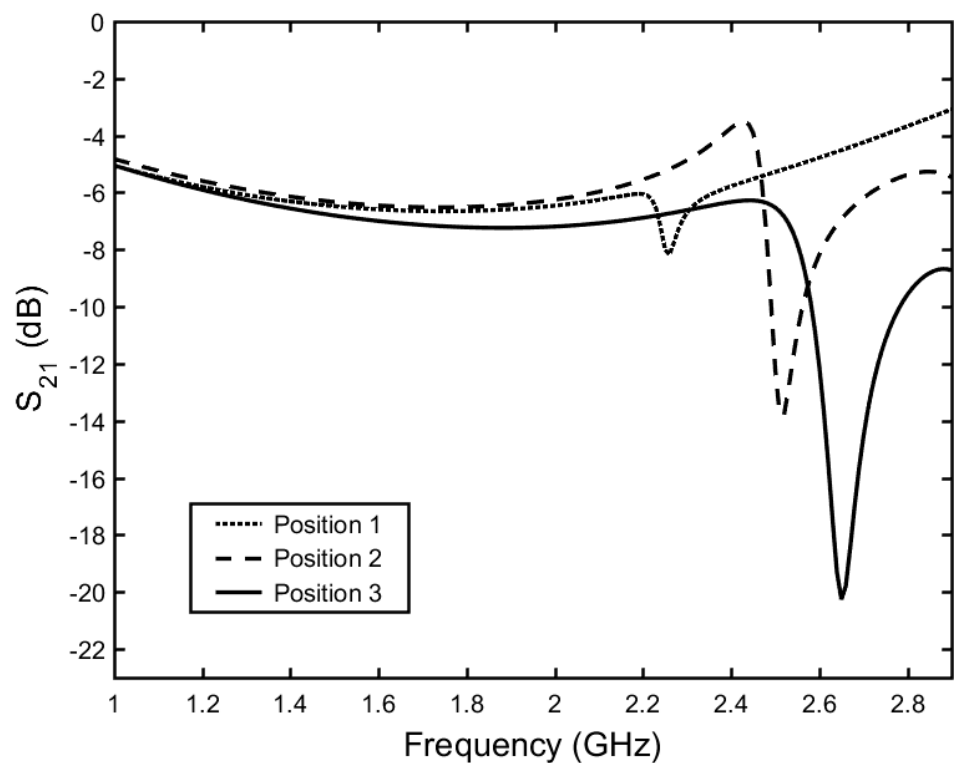


Figure 5. Simulated results of the transmission coefficient (S_{21}) for three different CSRR element positions on the microstrip planar circuit patch.

Figure 6 shows the simulated results for the circuit with and without the CSRR. In this work, the sensor is proposed with the CSRR element in position 3.

It can be observed in Figure 5 that the slotted CSRR element generated resonance close to 2.6 GHz in the sensor. This resonance is the parameter responsible for describing the dielectric characteristics of the materials analyzed in this work. The quality factor can be defined as $Q = f_r / \Delta f_{3dB}$, where f_r is the resonance frequency of the proposed sensor and Δf_{3dB} is the 3 dB bandwidth. With the resonance frequency of 2.65 GHz, shown in Figure 6, the proposed sensor has a quality factor of 53.97.

Therefore, based on the simulated results, the proposed sensor's operating range is located between 2 and 3 GHz, a range that meets different technologies and applications. As shown in Figure 7, we can observe that the operating frequency of the device in the unloaded state, and with the presence of the MUT, is within the range of widely used commercial applications.

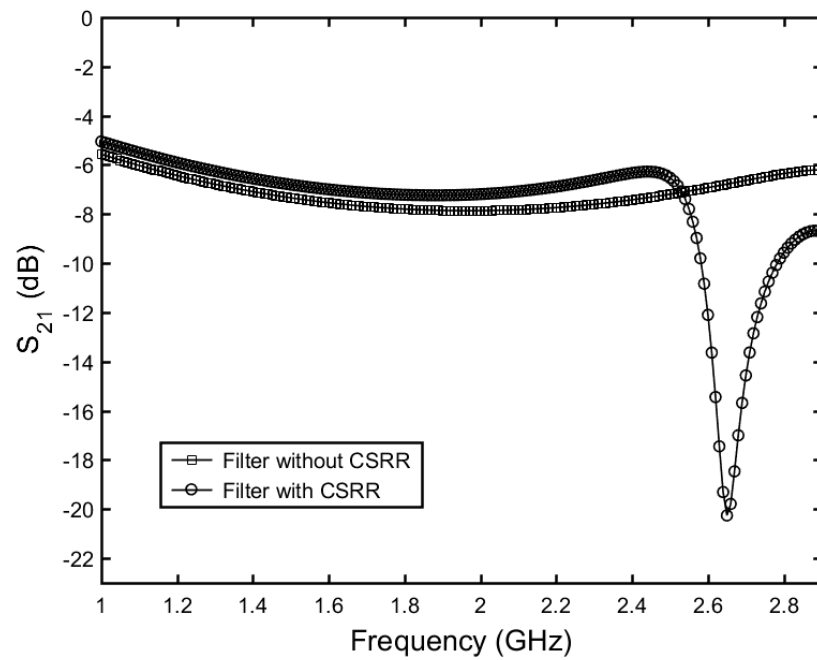


Figure 6. Simulated results of the proposed planar circuit without and with the CSRR element.

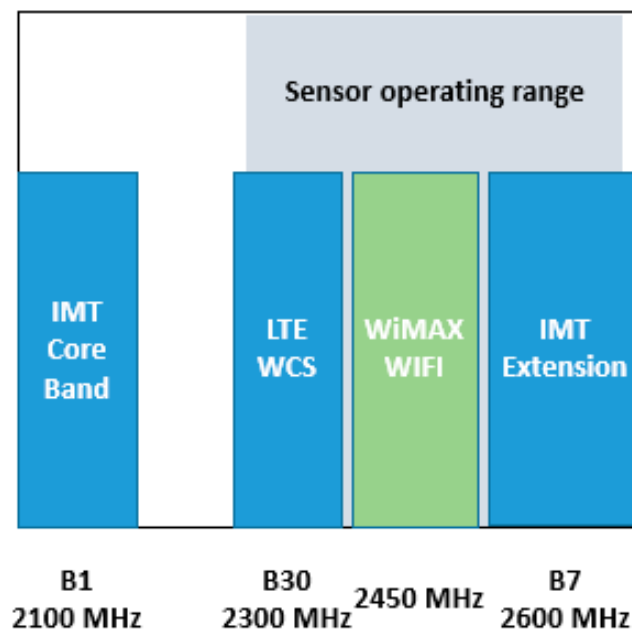


Figure 7. Frequency division LTE bands, compiled from 3GPP 36.101 [25].

In this way, the measurement of materials with electrical characteristics with higher values, above 9, is outside the operating range proposed in the work, as the operating frequency with this result would not meet the applications presented.

3. Results and Discussion

Two MUTs (FR-4 and glass) with equal dimensions (20 mm × 20 mm × 2 mm) are positioned on the patch, and their impact on the transmission coefficient (S_{21}) is shown in Figure 8. The permittivity value found in the literature for the FR-4 is $\epsilon_r = 4.4$. The permittivity of ϵ_r (glass) varies from 5 to 10, depending on its chemical composition; however, in microwave circuits, the value 5.5 is usually used [3].

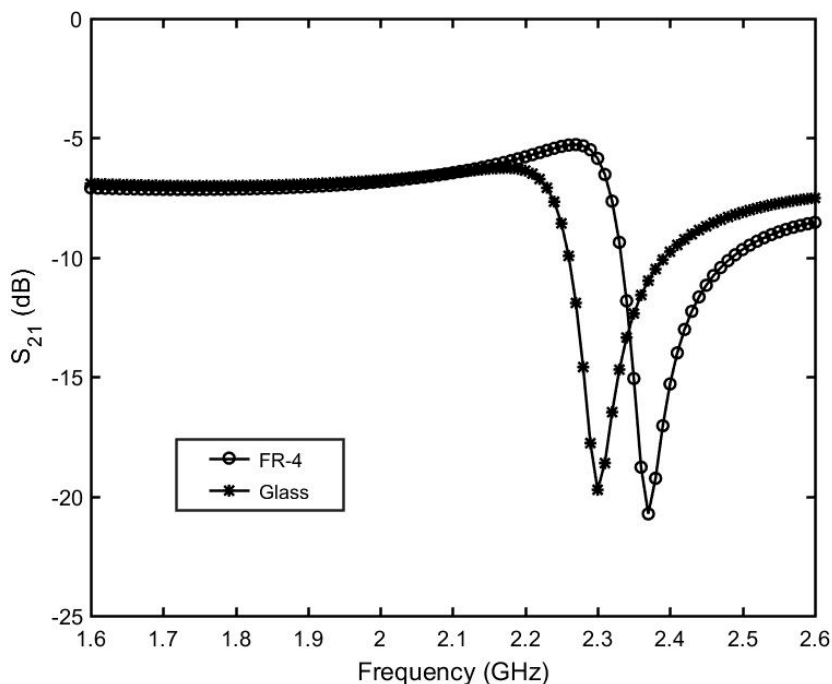


Figure 8. Transmission coefficient (S_{21}) simulated results as a function of the resonance frequency of the sensor for different MUTs.

The simulated results of the sensor show frequency responses for the two MUTs, which are 2.37 GHz for the FR-4 and 2.3 GHz for the glass. From Figure 8, it can be observed that the frequency decreases with the increased permittivity of the analyzed material, due to the disturbance suffered.

Simulations were performed with some values of ϵ_r (MUT) being fixed at $\tan \delta = 0$, within a frequency range. With these simulated results, it was possible to verify the sensitivity performance of the proposed sensor, shown in Figure 9, according to Equation (2). The frequency and the corresponding permittivity were used to obtain, through polynomial regression, the curve that describes the variation in the resonance frequency for specific ϵ_r values. Figure 10 shows the fitted curve for the simulated results within the analyzed frequency range.

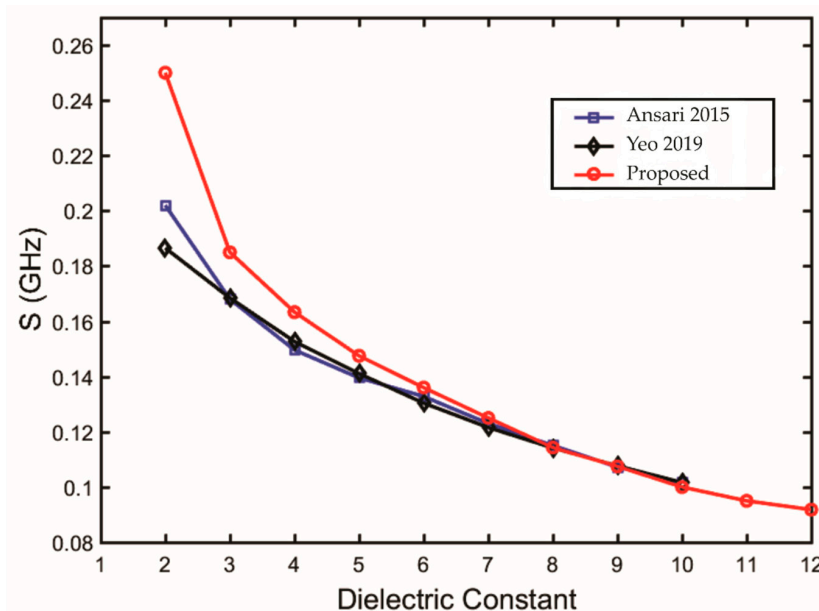


Figure 9. Results of the sensitivity parameter of the proposed sensor.

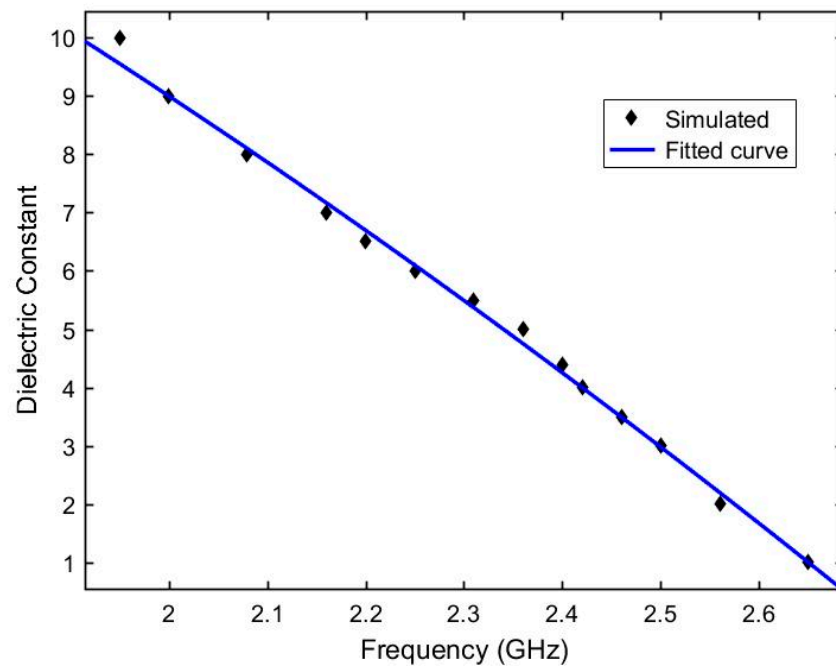


Figure 10. Simulated results and curve fitting for permittivity variation as a function of frequency.

Figure 9 shows that the sensitivity is not linear, in relation to permittivity. It presents higher values for smaller permittivity and decreases with the increase in the permittivity substrate values. When the MUT permittivity is $\epsilon_r = 2$, the sensitivity has a maximum value of 0.25 GHz, within the range of ϵ_r values analyzed. For the same value of ϵ_r , the sensitivity found in [14,23] is 0.202 GHz and 0.186 GHz, respectively. In $\epsilon_r = 3$, greater sensitivity variation is shown, decreasing from 0.25 GHz to 0.185 GHz, in the proposed sensor.

With the values obtained in Figure 10, it was possible to obtain the second-degree polynomial equation, shown in (6), with the determination coefficient $R^2 = 0.9952$.

$$\epsilon_r = -1.752f_{r,MUT}^2 - 4.161f_{r,MUT} + 24.33 \tag{6}$$

The MUT is positioned over the CSRR, where there is a greater concentration of electric field E in the resonance; however, despite having a larger field E, the magnetic field H is not null in the detection area, and has a small influence on the sensor quality [15]. Figure 11 shows the distribution of fields on the sensor surface at resonance. Thus, the quality factor is influenced by the tangent of electrical losses, the tangent of magnetic losses and the relative permittivity. Figure 12 shows the tangent of electrical losses as a function of the inverse normalized quality factor $|Q|^{-1}$ for small values of tangent of magnetic losses and permittivity $\epsilon_r = 1$.

With values of electric loss tangents and $|Q|^{-1}$ found for different relative permittivities and magnetic losses of tangent, Equation (7) was obtained, through curve fitting, for the electric loss tangent as a function of these parameters.

$$\tan\delta_e = p_1 + p_2 \tan\delta_m + \frac{p_3}{Q_n} + p_4 \tan\delta_m^2 + \frac{p_5 \tan\delta_m}{Q_n} + \frac{p_6}{Q_n^2} \tag{7}$$

where Q_n is the normalized quality factor and p_1, p_2, p_3, p_4, p_5 and p_6 are equations in terms of the relative permittivity, ϵ_r , obtained using (6):

$$p_1 = (2.238 \times 10^{-2} \epsilon_r^2 + 1.878 \epsilon_r + 72.89) \times 10^{-3} \tag{8}$$

$$p_2 = (-5.739 \epsilon_r^2 + 327.2 \epsilon_r - 1542) \times 10^{-3} \tag{9}$$

$$p_3 = \left(-4.696 \times 10^{-2} \varepsilon_r^2 + 2.675 \varepsilon_r - 80.32\right) \times 10^{-3} \tag{10}$$

$$p_4 = \left(-11.01 \times 10^{-2} \varepsilon_r^2 + 8.689 \varepsilon_r - 59.23\right) \tag{11}$$

$$p_5 = \left(-1.553 \varepsilon_r^2 + 88.18 \varepsilon_r - 1334\right) \times 10^{-3} \tag{12}$$

$$p_6 = \left(-1.235 \times 10^{-2} \varepsilon_r^2 + 0.6994 \varepsilon_r + 14.64\right) \times 10^{-3} \tag{13}$$

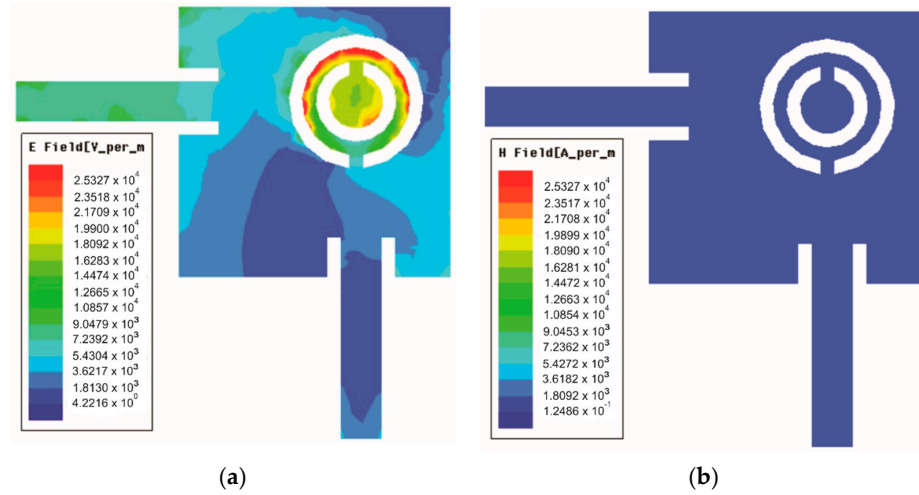


Figure 11. Field distribution on the sensor surface: (a) E and (b) H.

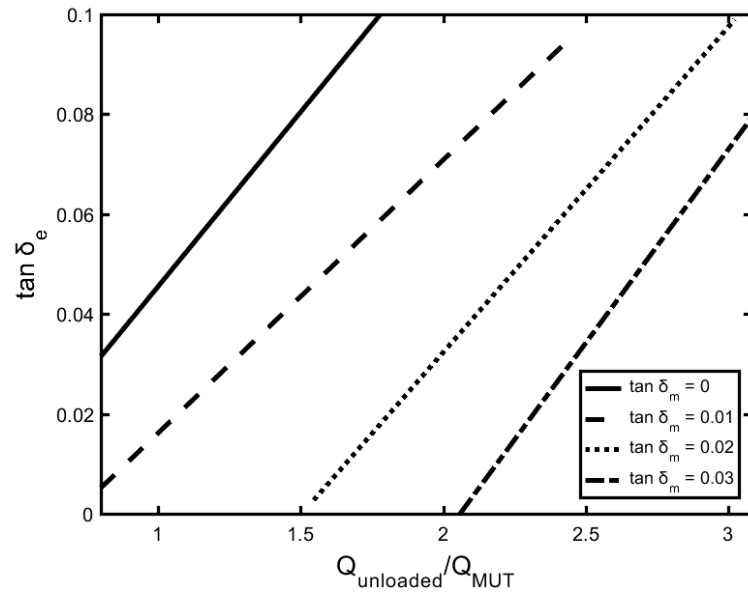


Figure 12. Results of the electric loss tangent as a function of the inverse normalized quality factor for different values of magnetic loss tangent.

Figure 13a shows a photograph of the proposed sensor prototype. Figure 13b shows the assembled structure with the sensor prototype, cables, connectors and a sample of the MUT, placed over the CSRR element, corresponding to the loaded case with FR-4. The measured results are shown in Figure 14a for both unloaded (air) and loaded (with FR-4 and glass) geometries. A comparison between the simulated and measured results for the geometries loaded with FR-4 and glass is shown in Figure 14b. Measurement results were obtained for both geometries using an E5071C vector network analyzer (VNA).

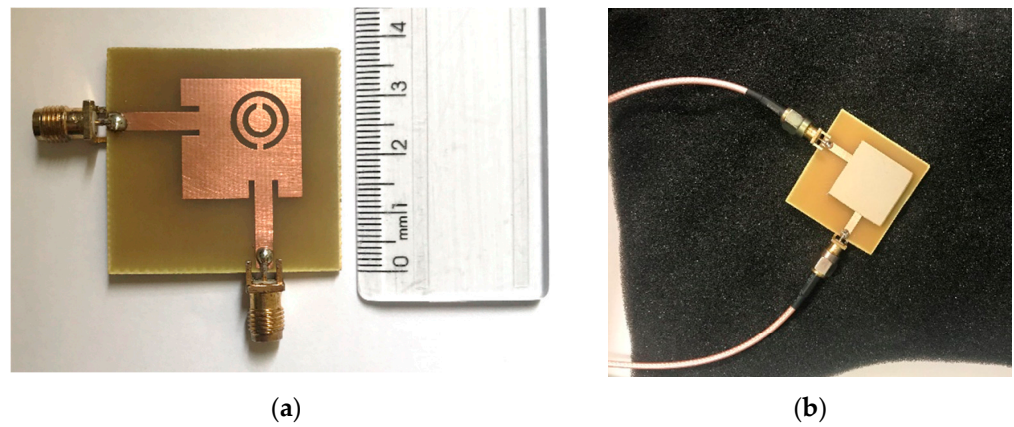


Figure 13. Photos of the (a) sensor prototype and (b) sensor geometry with an FR-4 MUT sample over the CSRR region.

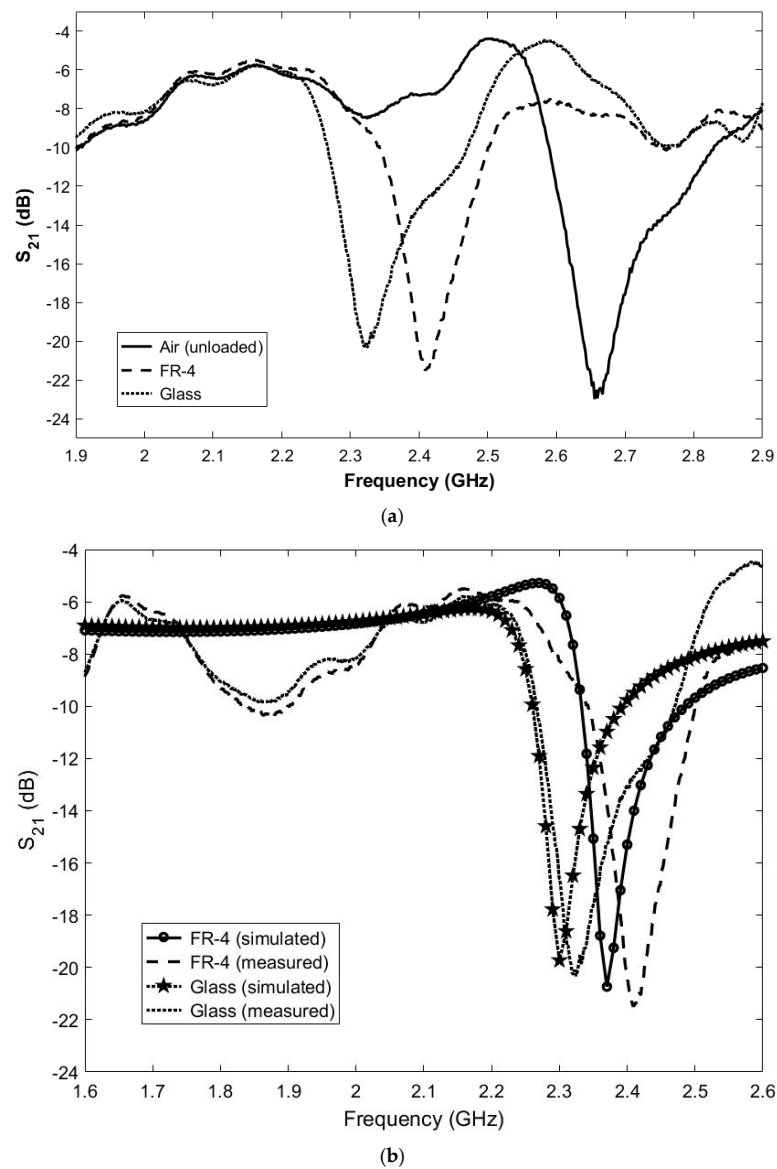


Figure 14. (a). Measured results of the transmission coefficient (S_{21}) for unloaded and loaded sensor geometries. (b). Simulated and measured results of the transmission coefficient (S_{21}) for the sensor geometries loaded with FR-4 and glass MUT samples.

The measured results shown in Figure 14b are due to the insertion of the FR-4 and glass materials on the CSRR. The resonance frequencies with the disturbance of these materials are 2.4 GHz and 2.31 GHz for the FR-4 and the glass, respectively. The simulated and measured results showed small relative differences, as shown in Table 2.

Table 2. Simulated and measured results for MUTs.

| MUT | Simulated Resonance Frequency (GHz) | Measured Resonance Frequency (GHz) | Difference (%) |
|-------|-------------------------------------|------------------------------------|----------------|
| Air | 2.65 | 2.645 | 0.19 |
| FR-4 | 2.37 | 2.4 | 1.25 |
| Glass | 2.30 | 2.31 | 0.43 |

The resonance frequency values obtained in Figure 14 were used as input parameters in Equation (6); in this way, it was possible to determine the dielectric constant of the analyzed materials (MUT). The dielectric constant found, as well as the normalized quality factor and the magnetic loss tangent obtained in Figure 12, were used as input parameters in Equation (7), to determine the electric loss tangent of the analyzed materials (MUT). Table 3 presents the obtained values and a comparison to those available in the literature.

Table 3. This work dielectric constant and loss tangent results compared to those available in the literature.

| MUT | ϵ_r | | $\tan \delta_e$ | | Difference (%) | |
|-------|--------------|-----------------------|-----------------|--------------------|----------------|-----------------|
| | This Work | Literature | This Work | Literature | ϵ_r | $\tan \delta_e$ |
| FR-4 | 4.25 | 4.3–4.4 [10,11,15] | 0.0198 | 0.02 [10,11,15] | 1.18 | 1.01 |
| Glass | 5.37 | 5.5 [3,11] | 0.0296 | 0.03 [8] | 2.42 | 1.35 |

Table 3 compares the values of ϵ_r and $\tan \delta_e$ obtained with the values found in the literature. The 2.4 GHz frequency obtained with the FR-4 material made it possible to determine a dielectric constant of 4.25, with a relative difference of 1.18%. The glass sample had a measured resonance frequency of 2.31 GHz and a calculated dielectric constant of 5.37, with a relative difference of 2.42%. From Equation (7), the electric loss tangent was obtained for different materials: $\tan \delta_e(\text{FR-4}) = 0.0198$ and $\tan \delta_e(\text{glass}) = 0.0296$, with relative differences of 1.01% and 1.35%, respectively. The results show good agreement and small values of relative differences for all cases.

Table 4 presents a comparison between the proposed sensor and those reported in the literature. The works mentioned have operating frequencies in the same frequency range of this work and with samples of dielectrics with relative permittivity, in greater quantity, below six. This frequency range was sought because it is of great interest today, mainly in the sub-6 GHz applications from 5G, Wi-Fi, WiMAX, Bluetooth and ISM, all with operating frequencies above 2 GHz (the range of interest in this work). For a better comparison with the works mentioned, the normalized sensitivity is used, given by Equation (3). For the proposed sensor, the normalized sensitivity is 4.82%. In fact, the proposed sensor is compact and has a great sensitivity value and an excellent maximum error (%), compared to the others.

Table 4. Comparison between results of the proposed sensor and other sensors reported in the literature.

| Ref. | Reson. Type | Meas. Reson. Freq. (GHz) | Size (mm × mm) | Sens. Param. | S (MHz) | $S_f(\%)$ | Complex Permitt. | Max. Error (%) |
|------|-------------------|--------------------------|----------------|--------------|---------|-----------|------------------|----------------|
| [5] | SIW cavity reson. | 2.188 | 55 × 50 | S21 | 8.1 | 0.368 | Yes | 3.24 |
| [14] | CSRR | 2.65 | 40 × 26 | S21 | 105.5 | 3.98 | Yes | 3.84 |
| [15] | CSRR | 2.461 | N/A | S21 | 42.2 | 1.71 | Yes | 1.56 |

Table 4. Cont.

| Ref. | Reson. Type | Meas. Reson. Freq. (GHz) | Size (mm × mm) | Sens. Param. | S (MHz) | S_f (%) | Complex Permitt. | Max. Error (%) |
|-----------|-------------------|--------------------------|----------------|--------------|---------|-----------|------------------|----------------|
| [18] | SRR | 2.41 | N/A | S21 | 72 | 3.63 | No | 3.6 |
| [19] | IDC | 3.316 | 40 × 50 | S21 | 166 | 5.05 | No | 14.01 |
| [23] | Meander-line slot | 2.5 | 80 × 80 | S11 | 102 | 4.06 | No | 2.68 |
| This Work | CSRR | 2.65 | 37 × 37 | S21 | 128 | 4.82 | Yes | 2.42 |

4. Conclusions

A new microwave planar two-port circuit structure, as a sensor, was developed to characterize the complex permittivity of dielectric materials, based on a CSRR inserted in the circuit patch. The principle of the sensor was the variation in the resonance frequency obtained when inserting the sample (MUT) over the CSRR region. Simulations were performed to determine the best location of the CSRR in the patch, to determine the resonance frequencies of the samples and to obtain a mathematical model to calculate the relative permittivity of the samples, from the resonance frequencies, and to calculate the loss tangent, according to the normalized quality factor, with the calculated relative permittivity and the contribution of the magnetic loss tangent. Good results were also obtained for sensitivity, with its best performance mainly in the range of low permittivity values. The experimental analysis was performed with the dielectric materials FR-4 and glass, which have dielectric constants and loss tangents typically known in the literature. The results showed small values of relative difference between the simulated and measured resonance frequencies, in addition to good agreement between the dielectric constants and the electric loss tangents calculated with those found in the literature, proving their usefulness for this purpose. The proposed sensor is compact, easy to fabricate and allows the possibility of application in other areas, such as the biomedical and industrial fields.

Author Contributions: J.K.A.N. contributed the idea, simulation, analysis, measurements, and paper writing, J.G.D.O. contributed on analysis, the measurements and paper writing, S.B.P. contributed the analysis and paper writing, V.P.S.N. assisted in the work development, A.G.D. contributed the idea, data analysis, and assisted in the work development and paper writing. All authors have read and agreed to the published version of the manuscript.

Funding: This research received no external funding.

Acknowledgments: This work was supported by CNPq under covenant 573939/2008-0 (INCT-CSF), CAPES and Federal University of Rio Grande do Norte (UFRN).

Conflicts of Interest: The authors declare no conflict of interest.

References

- Jilani, M.T.; Wen, W.P.; Cheong, L.Y.; Rehman, M.Z.U. A Microwave ring-resonator sensor for non-invasive assessment of meat aging. *Sensors* **2016**, *16*, 52. [[CrossRef](#)]
- Trabelsi, S.; Nelson, S.O. Microwave sensing of quality attributes of agricultural and food products. *IEEE Instrum. Meas. Mag.* **2016**, *19*, 36–41. [[CrossRef](#)]
- Li, Q.L.; Cheung, S.W.; Wu, D.; Yuk, T.I. Optically transparent dual-band MIMO antenna using micro-metal mesh conductive film for WLAN system. *IEEE Ant. Wirel. Propag. Lett.* **2016**, *16*, 920–923. [[CrossRef](#)]
- Kumari, R.; Patel, P.N.; Yadav, R. An ENG-inspired microwave sensor and functional technique for label-free detection of aspergillus niger. *IEEE Sens. J.* **2018**, *18*, 3932–3939. [[CrossRef](#)]
- Wei, Z.; Huang, J.; Li, J.; Xu, G.; Ju, Z.; Liu, X.; Ni, X. A High-sensitivity microfluidic sensor based on a substrate integrated waveguide re-entrant cavity for complex permittivity measurement of liquids. *Sensors* **2018**, *18*, 4005. [[CrossRef](#)] [[PubMed](#)]
- Chretiennot, T.; Dubuc, D.; Grenier, K. A microwave and microfluidic planar resonator for efficient and accurate complex permittivity characterization of aqueous solutions. *IEEE Trans. Microw. Theory Tech.* **2012**, *61*, 972–978. [[CrossRef](#)]

7. Ebrahimi, A.; Scott, J.; Ghorbani, K. Ultrahigh-Sensitivity Microwave Sensor for Microfluidic Complex Permittivity Measurement. *IEEE Trans. Microw. Theory Tech.* **2019**, *67*, 4269–4277. [[CrossRef](#)]
8. Nitsche, R.G.; Preissner, J.; Biebl, E.M. A free space technique for measuring the complex permittivity and permeability in the millimeter wave range. In Proceedings of the 1994 IEEE MTT-S International Microwave Symposium Digest, San Diego, CA, USA, 23–27 May 1994; pp. 1465–1468.
9. Wu, J.; Wang, P.; Huang, X.J.; Rao, X.F.; Chen, X.; Shen, Z.; Yang, H. Design and validation of liquid permittivity sensor based on RCRR microstrip metamaterial. *Sens. Actuators A Phys.* **2018**, *280*, 222–227. [[CrossRef](#)]
10. Boybay, M.S.; Ramahi, O.M. Material characterization using complementary split-ring resonators. *IEEE Trans. Instrum. Meas.* **2012**, *61*, 3039–3046. [[CrossRef](#)]
11. Oliveira, J.G.D.; Pinto, E.N.M.G.; Silva Neto, V.P.; D’Assunção, A.G. CSRR-based microwave sensor for dielectric materials characterization applied to soil water content determination. *Sensors* **2020**, *20*, 255. [[CrossRef](#)]
12. Ebrahimi, A.; Withayachumnankul, W.; Al-Sarawi, S.; Abbott, D. High-sensitivity metamaterial-inspired sensor for microfluidic dielectric characterization. *IEEE Sens. J.* **2013**, *14*, 1345–1351. [[CrossRef](#)]
13. Tiwari, N.K.; Singh, S.P.; Akhtar, M.J. Novel Improved sensitivity planar microwave probe for adulteration detection in edible oils. *IEEE Microw. Wirel. Comp. Lett.* **2019**, *29*, 164–166. [[CrossRef](#)]
14. Ansari, M.A.H.; Jha, A.K.; Akhtar, M.J. Design and application of the CSRR-based planar sensor for noninvasive measurement of complex permittivity. *IEEE Sens. J.* **2015**, *15*, 7181–7189. [[CrossRef](#)]
15. Saadat-Safa, M.; Nayyeri, V.; Khanjarian, M.; Soleimani, M.; Ramahi, O.M. A CSRR-based sensor for full characterization of magneto-dielectric materials. *IEEE Trans. Microw. Theory Tech.* **2019**, *67*, 806–814. [[CrossRef](#)]
16. Fan, L.; Zhao, W.; Gan, H.; He, L.; Liu, Q.; Dong, L.; Wang, G. A high-Q active substrate integrated waveguide based sensor for fully characterizing magneto-dielectric (MD) materials. *Sens. Actuators A Phys.* **2020**, *301*, 111778. [[CrossRef](#)]
17. Zhao, W.; Gan, H.; He, L.; Liu, Q.; Wang, D.; Xu, K.; Chen, S.; Dong, L.; Wang, G. Microwave planar sensors for fully characterizing magneto-dielectric materials. *IEEE Access* **2020**, *8*, 41985–41999. [[CrossRef](#)]
18. Ebrahimi, A.; Scott, J.; Ghorbani, K. Differential Sensors Using Microstrip Lines Loaded with Two Split-Ring Resonators. *IEEE Sens. J.* **2018**, *18*, 5786–5793. [[CrossRef](#)]
19. Kapoor, A.; Varshney, P.K.; Akhtar, M.J. Interdigital capacitor loaded electric-LC resonator for dielectric characterization. *Microw. Opt. Technol. Lett.* **2020**, *62*, 1–6. [[CrossRef](#)]
20. Ali, L.; Wang, C.; Ullah, I.; Yousaf, A.; Khan, W.U.; Ullah, S.; Khan, R.; Alassery, F.; Hamam, H.; Shafiq, M. Design and Optimization of Microwave Sensor for the Non-Contact Measurement of Pure Dielectric Materials. *Electronics* **2021**, *10*, 3057. [[CrossRef](#)]
21. Chen, S.; Guo, M.; Xu, K.; Zhao, P.; Dong, L.; Wang, G. A Frequency synthesizer based microwave permittivity sensor using CMRC structure. *IEEE Access* **2018**, *6*, 8556–8563. [[CrossRef](#)]
22. Ebrahimi, A.; Scott, J.; Ghorbani, K. Transmission Lines Terminated with LC Resonators for Differential Permittivity Sensing. *IEEE Microw. Wirel. Comp. Lett.* **2018**, *28*, 1149–1151. [[CrossRef](#)]
23. Yeo, J.; Lee, J.-I. Meander-line slot-loaded high-sensitivity microstrip patch sensor antenna for relative permittivity measurement. *Sensors* **2019**, *19*, 4660. [[CrossRef](#)] [[PubMed](#)]
24. Vélez, P.; Muñoz-Enano, J.; Ebrahimi, A.; Herrojo, C.; Paredes, F.; Scott, J. Single-Frequency Amplitude-Modulation Sensor for Dielectric Characterization of Solids and Microfluidics. *IEEE Sens. J.* **2021**, *21*, 12189–12201. [[CrossRef](#)]
25. 3GPP TS 36.101. Evolved Universal Terrestrial Radio Access (E-UTRA). In *User Equipment (UE) Radio Transmission and Reception (Release 15)*; ETSI: Sophia Antipolis, France, 2019.